REPORT:

Authors:
Lawrence A. Shepp *is a member of technical staff in the Mathematics Research Department at AT&T Bell Laboratories in Murray Hill, New Jersey. He does research in mathematics and tomography. Mr. Shepp joined AT&T in 1962. He has a B.S. in applied mathematics from the Polytechnic Institute of New York, and both a B.A. and Ph.D. in mathematics from Princeton University.*
Sushanta Srivastava *is a member of technical staff in the Digital Transmission Services Planning Department at AT&T Bell Laboratories in Holmdel, New Jersey. Mr. Srivastava joined AT&T in 1978. He has a B.Sc. in physics from Delhi University, a B.S.E.E. from the Indian Institute of Science, and an M.S.E.E. and a Ph.D. in electrical engineering from the University of Pennsylvania.*

COMPUTED TOMOGRAPHY OF PKM AND AKM EXIT CONES

Introduction

In February 1984, two shuttle-launched spacecraft, the Westar IV and Palapa B2 satellites, failed to reach orbit when their perigee kick motors (PKMs) extinguished in a few seconds, instead of burning for 86 seconds. Although the two failed PKMs could not be recovered, a television camera aboard the space shuttle Challenger had observed the premature extinction of the Palapa PKM.

Two failures in succession caused serious concern about the reliability of all subsequent spacecraft launches, including two AT&T Telstar 3 satellites that were to use PKMs with similar light, carbon-carbon exit cones (Figure 1).

Exit Cone Failure

Communications satellites like these are usually ejected from the space shuttle or other launch vehicle into a 100 to 400 nautical mile circular parking orbit. At a predetermined time and specified orientation after ejection, many fire an attached PKM (or AKM, apogee kick motor) that moves them through a transfer orbit to their geostationary orbit.

Before these two failures, all 18 launches using similar PKMs were successful. However, during test firings, a few of these PKMs had extinguished prematurely in a few seconds because their exit cones failed.

Although no direct evidence was found to explain the in-orbit failures, a large panel of experts surmised that the failures were caused by mechanical weaknesses resulting from fine-density variations or delaminations in the exit cones (Figure 2). To minimize the risks for future spacecraft launches that use these PKMs, it was essential to develop reliable methods for screening deficient exit cones.

After the in-orbit PKM failures, an additional procedure that involved computed tomography (CT) was used for screening the fabricated exit cones. As an X-ray beam scans a particular plane of the exit cone, digital signals about the degree of radiation absorbed are transformed by a computer into a cross-sectional image; other planes are not involved. However, because CT cannot accurately image objects that are finer than its resolution, its ability to reveal fine-density variations or delaminations that could cause PKM failures had not been established.

Through computer simulations, we show that CT can indicate the presence of these fine defects because of its *tangent-casting effect* associated with sharp, material density variations (see Panel 1, page 84). Therefore, if exit-cone CT images are judiciously interpreted, we believe CT can enhance the reliability of exit-cone screening and reduce the risks of using PKMs with carbon-carbon exit cones for spacecraft launches.

Density Variations

The failed PKMs used short carbon-carbon exit cones (Figure 1). The cone, which is 20 mm thick, is assembled (Figure 3) from six *rosette* subassemblies. Each subassembly consists of 60 layers of carbon-carbon cloth

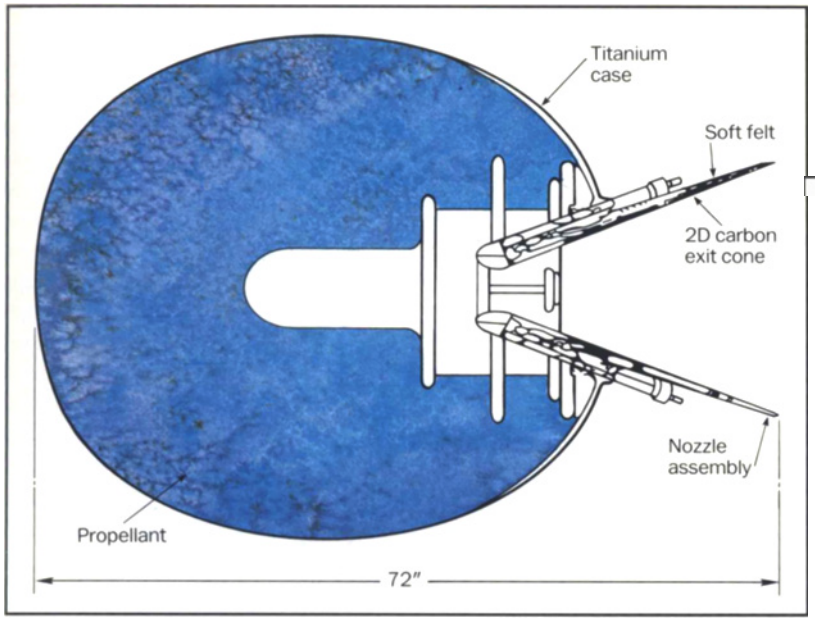

Figure 1. Cross-section of PKM and exit cone.

(Figure 4) that are overlapped at the joints to form the cone. A carbon-carbon exit cone typically weighs 5.5 kg (as compared to 13 to 18 kg for the older carbon-phenolic design).

Carbon-carbon exit cones are carbonized to increase density and pyrolized to 2200°C to improve consistency and mechanical properties. To further increase density, carbon is deposited for 150 hours through chemical vapor deposition (CVD) with methane. The CVD is repeated if the density is too low; 1.4

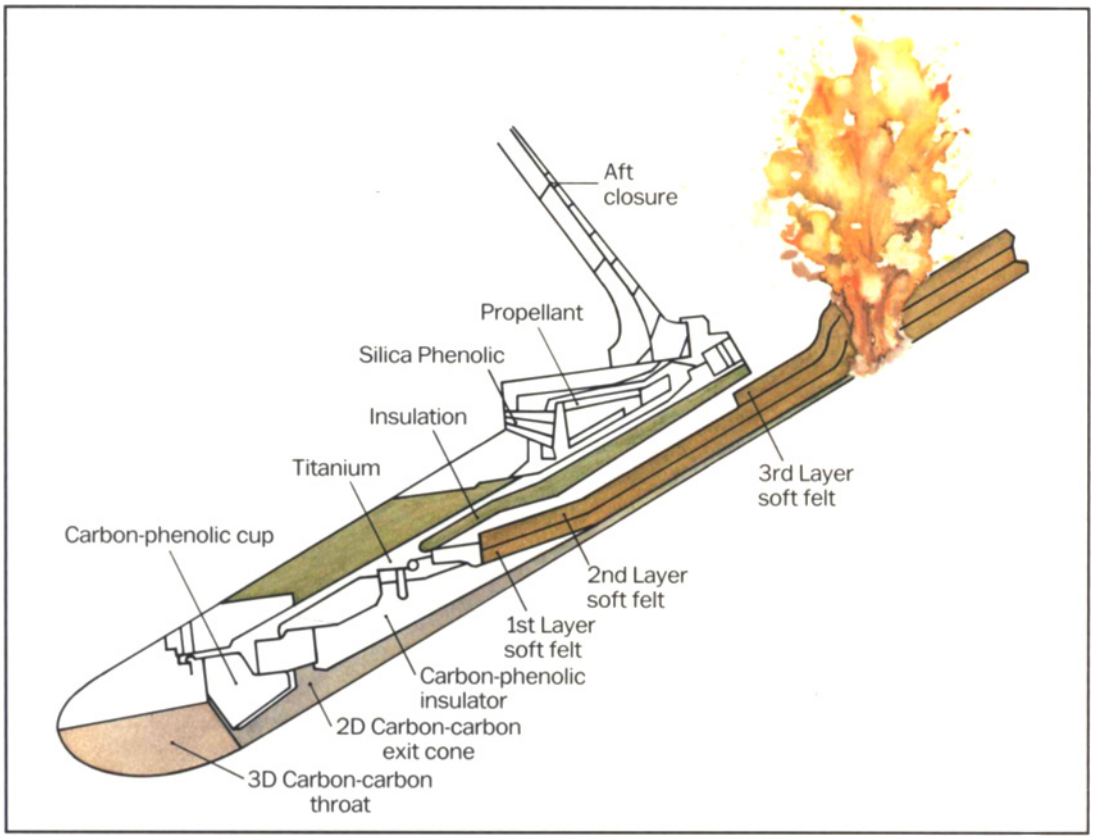

Figure 2. Surmised failure of exit cone.

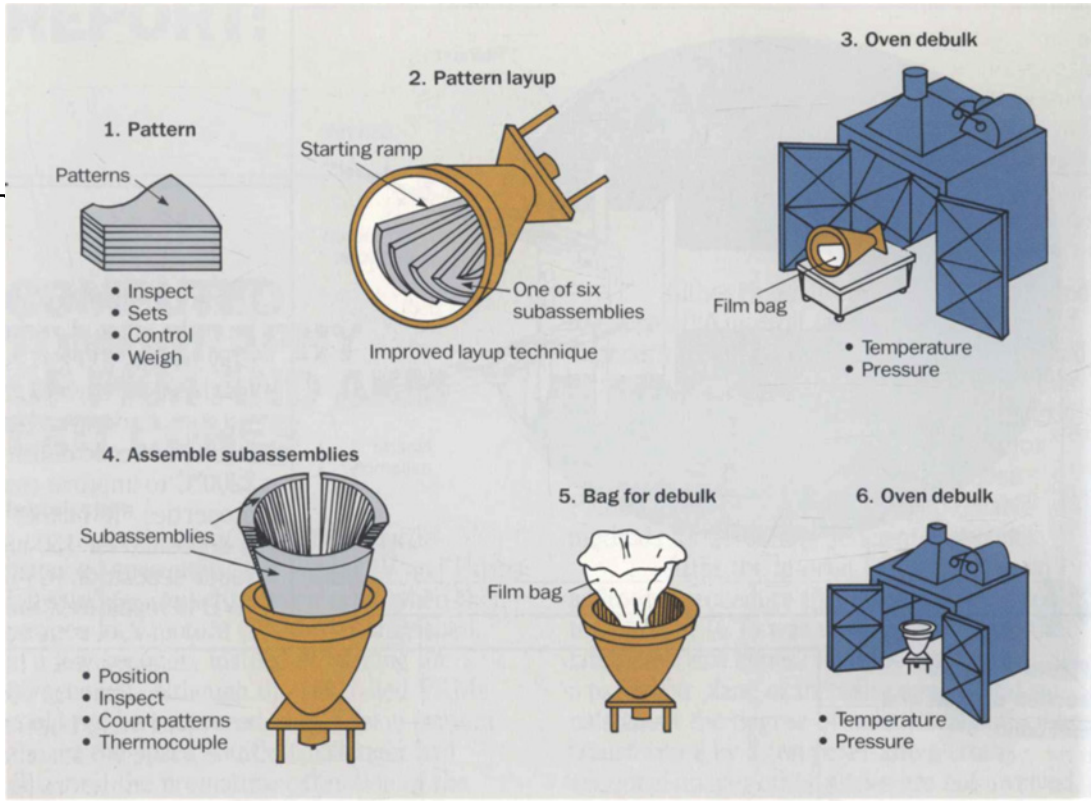

Figure 3. Procedure for fabricating an exit cone.

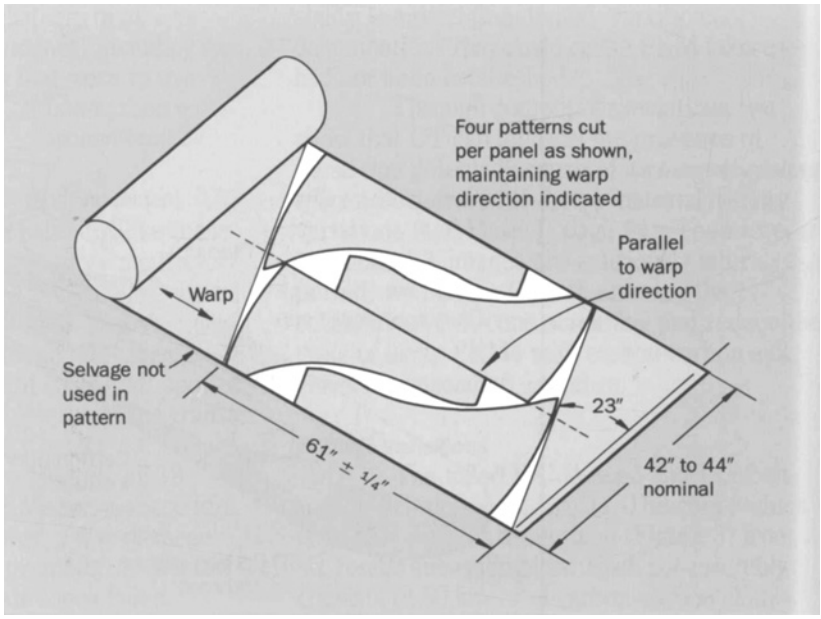

Figure 4. Cloth is cut to form the cone.

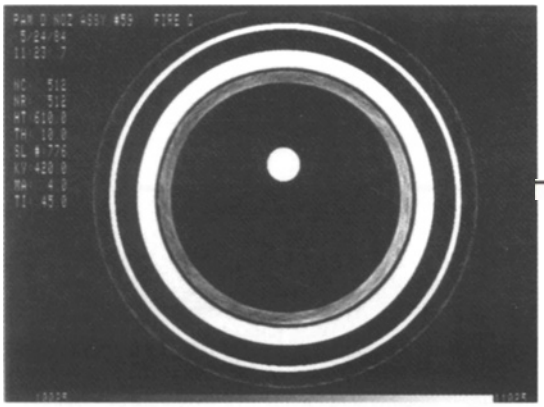

Figure 5. CT cross section. Inner annulus is the carbon-carbon cone, and the next annulus is the titanium housing. The small circle is the Teflon® rod to normalize the CT values. The run data on the left shows the cone number (this is the Telstar 3 cone), and height (HT) in millimeters of the slice plane above the base of the cone. This image does not show delaminations, although there are density variations. *("Teflon" is a registered trademark of E.I. duPont de Nemours & Co.)*

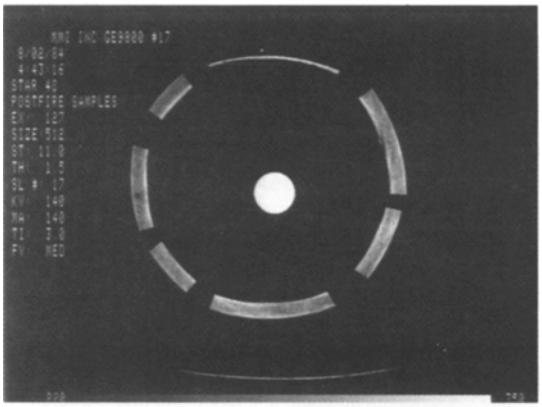

Figure 6. A composite of several sawed-off pieces of cones scanned with a medical CT scanner that could be used only when there is no titanium housing. Note the obvious delamination at 2 o'clock and decreased density at 9 o'clock.

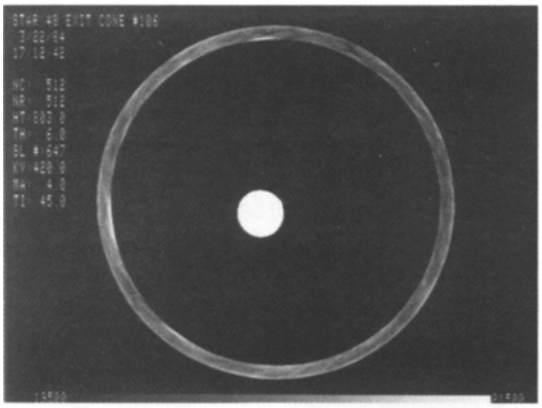

Figure 7. This section of rejected cone, shows an artifact at 8 o'clock.

to 1.55 g/cc is acceptable.

Despite extensive quality control, X-ray examination, ultrasonic evaluation and other inspection techniques used during manufacturing, there are considerable uncertainties about the mechanical properties of the finished exit cone.

This prompted a return to carbon-phenolic exit cones, because they are considered more forgiving of material defects and have a greater margin of safety. However, PKMs (or AKMs) now must move these heavier cones. For shuttle-launched Telstar 3 type missions, the spacecraft weight penalty during transfer orbit could be as high as 8 kg, resulting in a 7.5-month decrease in in-orbit spacecraft life.

Two factors led AT&T to decide to proceed with the August 1984 Telstar 3 launch using a carbon-carbon cone (which turned out to be successful). First, if the Telstar 3 satellite was to use a PKM with the carbon-phenolic exit cone, the earliest possible launch was March 1985. Second, the CT scan of the carbon-carbon cone that would be used revealed no defects, although defects (Figure 6) were seen in other carbon-carbon cones with CT.

However, considerable controversy remained about the reliability of these carbon-carbon exit cones. Because of these controversies, the Telstar 3 successfully launched in June 1985 used a PKM with a carbon-phenolic exit cone.

At first, the inherent resolution of CT would seem to be inadequate to image a delamination of only one laminar cloth layer. This layer is only 1/60 the overall thickness of 20 mm, and the 0.4 mm ray-spacing distance between adjacent measurements with the CT device used (at Aerojet Corporation, Sacra-

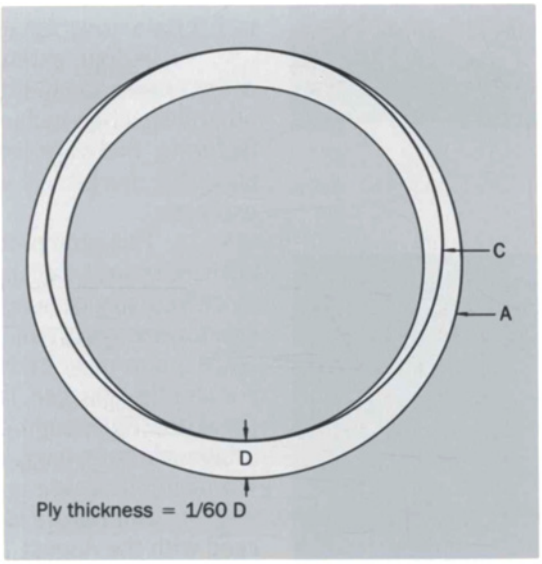

Figure 8. In this simulated exit-cone slice, A is the carbon-carbon cone, and C is a delamination.

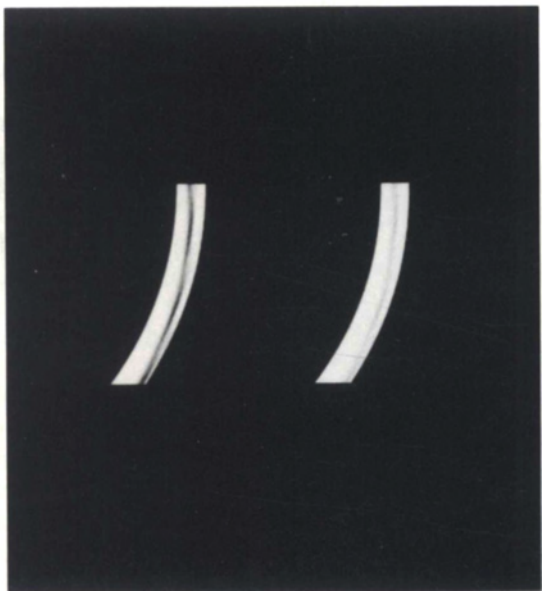

Figure 9. Reconstruction of one section of simulated cone.

mento, California) is about six times coarser.

Nevertheless, because the delaminations are likely to appear as curves rather than as isolated points, we felt the CT would image the small density variations that occur along such a laminar fault curve.

The reason for this was the well-known artifact in CT that causes casting of lines that are tangent to dense or hollow objects. An artifact is a flaw in the image caused by either the reconstruction algorithm or an error in the data acquired. Here, it is a result of the way the CT reconstruction algorithm uses back projection along lines[1] (see Panel 1, page 84).

For an exit-cone delamination, a tangent artifact might work to our advantage because it would trace the fault curve and enhance it. This was indeed true in the simulation study we made recently.

Simulating CT Results

Figure 5 shows a typical CT scan of one level of an exit cone. The interior annulus is the carbon-carbon cone. Although there are clear variations in density, this cone was judged acceptable after we looked at all slices (5 mm apart).

McDonnell-Douglas, the PKM manufacturer, used this CT criterion to reject a cone: If, in any slice, a region of decreased density (< 1.35 g/cc) follows the laminar lines (i.e., clockwise from inner to outer diameter) for at least 9 degrees, the cone is rejected.

In Figure 6, we can see a known delamination in a cut-up cone (that tests, other than CT, also rejected). Even visual inspection showed artifacts on the cone's inner surface.

Figure 7 shows a slice of a cone that was rejected by McDonnell-Douglas' criterion.

The question remained: How small a density variation over how narrow a laminar curve can be observed with a CT scan? Our simulation showed it should be possible to observe clearly a decreased density of 1.35 g/cc in a single laminar layer (see Panel 2, page 85).

We computed the X-ray measurement data for the mathematical phantom of Figure 8. A thin annulus C—that represents a delamination and has a density d—is tangent to both the inner and outer diameter of annulus A—that represents one section of the carbon-carbon cone.

Strip integration was used to calculate the (noise-free) X-ray measurement data, because it is easy to calculate the area of the intersection of an ellipse and an arbitrary strip. We took the thickness of C to be 1/60 of A's thickness and the density d of D to be 0 to 99 percent that of A.

As Figure 9 shows, C's identification is clear in the reconstruction of A when d is 0 percent on the left or 50 percent on the right. Other experiments showed that, even when d is 99 percent, it is possible to observe C in A, with noiseless data.

Although we can make statistical noise arbitrarily small by lengthening scan time, other sources of noise will limit such fine measurement.

Of course, a real delamination might be thicker than a single laminar layer (1/60 the width of A). It is important to observe that the reconstruction of C in Figure 9 shows C much thicker than it is in reality (i.e., the reconstruction is not quantitative). This also shows that an exact mathematical analysis is not possible because we are imaging the error or artifacts that result from the tangent-casting property of the reconstruction algorithm.

Conclusions

Despite CT's inability to image exit-cone delaminations accurately, the simulations show that delaminations can be clearly detected even in a single layer of the carbon-carbon cloth.

This evidence that CT can effectively discriminate delaminated and mechanically deficient cones should restore confidence in using CT to screen carbon-carbon exit cones. Returning to the use of the lighter carbon-carbon design would result in about 6 percent longer in-orbit life of the satellites.

Acknowledgments

The authors are grateful to P. G. Doyle and J.A. Reeds for discussions.

Reference

1. L. A. Shepp and B. F. Logan, "The Fourier Reconstruction of a Head Section," *IEEE Trans. Nucl. Sci.*, Vol. NS-21, 1974, pp. 21-43.

(Manuscript received November 14, 1985)

Although Reference 1 covers the tangent-casting effect in some detail, it is useful to amplify that discussion here for completeness and because the tangent-casting effect is so basic to computer tomography (CT).

The convolution-back-projection algorithm of CT reconstructs a density $f(x,y)$ by adding up the derivative of the Hilbert transform of the projection of f in each direction θ. Thus, if $P_f(t,\theta)$ is the line integral of f along a line that is t distance from zero in direction θ

$$P_f(t,\theta) = \int_{-\infty}^{\infty} f(t\cos\theta + s\sin\theta, -t\sin\theta + s\cos\theta)\, ds,$$

then one forms the derivative $Q_f(t,\theta)$ of the Hilbert transform of P_f

$$Q_f(t,\theta) = \int_{-\infty}^{\infty} P_f(t-u,\theta)\,\psi(u)\, du,$$

$$\hat{\psi}(w) = (-iw)\, i\, sgn(w) = |w|,$$

where $\hat{\psi}$ is the Fourier transform of ψ. Finally, f is reconstructed by

$$f(x,y) = \frac{1}{\pi}\int_0^{\pi} Q_f(x\cos\theta + y\sin\theta\,,\,\theta)\, d\theta\ .$$

Let's give an example that also shows the tangent-casting effect. Consider an ellipse with a density of one centered at the origin and with semiaxes α, β along the x and y axes, respectively. Also, let $f(x,y)$ equal one if the point (x,y) is inside the ellipse or zero if it is outside the ellipse.

Therefore,

$$f(x,y) = 1 \text{ if } \left(\frac{x}{\alpha}\right)^2 + \left(\frac{x}{\beta}\right)^2 \leq 1 \text{ and } f(x,y) = 0 \text{ otherwise.}$$

Then, the projections $P_f(t,\theta)$ are given by

$$P_f(t,\theta) = \frac{2\alpha\beta}{a^2(\theta)}\sqrt{a^2(\theta) - t^2}\,, \quad |t| \leq a(\theta)$$

$$P_f(t,\theta) = 0 \qquad\qquad , \quad |t| > a(\theta),$$

where $a^2(\theta) = \alpha^2\cos^2\theta + \beta^2\sin^2\theta$ is the square of the half-width in direction θ.

The derivative of the Hilbert transform of P_f is

$$Q_f(t,\theta) = \frac{2\alpha\beta}{a^2(\theta)}, \qquad |t| \leq a(\theta)$$

$$Q_f(t,\theta) = 2 - 2|t|(t^2 - a^2(\theta))^{-1/2}, \quad |t| > a(\theta).$$

Thus, $Q_f(t,\theta)$ is perfectly flat inside the projection of the support of f in direction θ. But, at distance $t = \pm(a(\theta) + \epsilon)$, i.e., just off the support, then $Q_f(t,\theta)$ is nearly $-\infty$. If we have a finite number of angles θ, as happens in practice, f is reconstructed by

$$f(x,y) = \frac{1}{N}\sum_{k=1}^{N} \tilde{Q}_f(X\cos\theta_k + y\sin\theta_k\,,\,\theta_k),$$

where $\tilde{Q}_f$ is an approximation to Q_f.

As such, $\tilde{Q}$ has large negative sidelobes just outside the support of f. These sidelobes propagate across the reconstruction and cause overshoot errors all along the tangent lines to the support of any ellipse. Also, there is a tangent-casting artifact in each of the N directions.

As N approaches ∞, these artifacts disappear; but, for a finite N, these straight-line artifacts remain and are commonly seen. They are usually an annoying disadvantage. But, when one looks for delaminations, the straight-line artifacts actually help enhance them.

We used the program *fullmdacs* (Figure A) to conduct the experiment that tested whether delaminations can be seen. The `read` statement reads the ellipse parameters of the four ellipses used (in reality, all are circles).

Thus, the point (xl, yl) is the center of the ellipse; $al = bl$ is the radius, and gl is incremental density. (To specify these ellipses, we did not need tl, which represents the tilt angle of the major axis of the ellipse used. Because we are using only circles, there is no major axis.)

As line 1 of *lumpmdacl* (Figure B) shows, the outer circle has a radius of 0.9 and density of 1, and is centered at (0, 0). The second circle is centered at (0, 0.04425) and has a radius of 0.85575 and incremental density of –1. The third circle, also centered at (0, 0.04425), has a radius 0.85425, while the fourth or inner circle is centered at (0, 0) and has a radius 0.81.

Thus, the second circle is tangent to the first circle or outside of the cone, and the third circle is tangent to the fourth circle or inside of the cone. This is an attempt to simulate a laminar layer of zero density.

Hence, the sum of the first two densities is zero inside the ellipse. Finally, the third and fourth ellipses (circles) add back to density 1 inside the annulus that the first and fourth circles defined.

Thus, the second and third ellipses effectively remove a single delamination in this simple model. As discussed in this paper, in later runs we decreased the effective delamination to 0.9 by setting $gl(l)$ to 1, –0.1, 0.1, –1 for l equals 1, 2, 3, 4.

The strip integrals are calculated and stored in the array $proj(j, k)$. For each direction of projection, the derivative of the Hilbert transform approximation is calculated and stored in the array *conv*. The reconstruction is calculated and stored in the array $z(i, l)$ that is finally gray-level coded and displayed, as in Figure 9.

Incidentally, except for the choices of ellipse parameters, this program is the same as the one Shepp and Logan used in Reference 1.

Figure A. Simulation program *fullmdacs* that was used to determine if delaminations are visible in CT scans.

```
c    nr=no. of rays/view;nv=no. of views;raywidth is width of strip
c    usually take raywidth=ar(strips abut).
       parameter (nv=100,nr=200,n=nv,m=nr,np=128,nl=4)
       dimension phi(m),proj(n,m),conv(m)
       dimension z(np,np),tk(nr)
       dimension xl(nl),yl(nl),al(nl),bl(nl),tl(nl),gl(nl)
       dimension e(nl),distl(nl),factor(nl)
       pi=atan(1.)*4.
       pin=pi/n
       ar=2./(m-1)
c  **********************************
       do 51 l=1,nl
       read(5,1002) xl(l),yl(l),al(l),bl(l),tl(l),gl(l)
1002   format(6f10.5)
       print 1101,l,xl(l),yl(l),al(l),bl(l),tl(l),gl(l)
1101   format(i3,6f10.5)
       factor(l)=al(l)*bl(l)*gl(l)
51     continue
c  **********************************
       do 31 k=1,m
       tk(k)=-1.+(k-1)*ar
31     continue
c  **********************************
       do 10 j=1,n
       thetaj=(j-1)*pin
       sinthtaj=sin(thetaj)
       costhtaj=cos(thetaj)
       raywidth=ar
       d=.5*raywidth
c  **********************************
       do 53 l=1,nl
       s=sin(thetaj-tl(l)*pi)
       c=cos(thetaj-tl(l)*pi)
       e(l)=(al(l)*c)**2+(bl(l)*s)**2
       distl(l)=xl(l)*costhtaj+yl(l)*sinthtaj
53     continue
c  **********************************
       do 22 k=1,m
       do 54 l=1,nl
       dist=tk(k)-distl(l)
       distp=dist+d
       distm=dist-d
       diffp=e(l)-distp**2
```

Figure A. ***continued***

```
      diffm=e(l)-distm**2
      if(diffp.le.0.and.diffm.le.0) go to 54
      yp=sqrt(amax1(0.,diffp))
      ym=sqrt(amax1(0.,diffm))
      pee=distp*yp-distm*ym
      pee=pee/e(l)+atan2(distp,yp)-atan2(distm,ym)
      proj(j,k)=proj(j,k)+pee*factor(l)/raywidth
54    continue
22    continue
1001  format(5f15.8)
10    continue
ccccccccccccccccccccccccccccccccccccccccccccccccccccc
      xpos-1.
      yneg=.5
      ypos=.5
      yneg=.0
      a=ar
      c2=-1/(*pi*n)
      deltax=(xpos-xneg)/np
      deltay=(ypos-yneg)/np
c  **********************************
      phi(1)=2/(pi*n)
      do 710 k=1,m-1
      phi(k+1)=c2/(k*k-.25)
710   continue
c  **********************************
      do 720 j=1,n
      thetaj=(j-1)*pin
      sinthtaj=sin(thetaj)
      costhtaj=cos(thetaj)
      cosdeloa=costhtaj*deltax/a
1066  format(i10,"   proj")
c  **********************************
      do 730 kr=1,m
      conv(kr)=0
      do 740 k=1,m
      kabs=iabs(kr-k)+1
      conv(kr)=conv(kr)+proj(j,k)*phi(kabs)/a
740   continue
730   continue
c  **********************************
1007  format(i10,4f15.8,"   conv")
      do 751 iy=1,np
```

Figure A. ***continued***

```
      y1=yneg+(iy-.5)*deltay
      r=1.+(1./a)+((xneg-.5*deltax)*costhtaj+sinthtaj*y1)/a
      do 750 ix=1,np
      r=r+cosdeloa
      l=r
      if(l.le.0.or.l.ge.m) go to 750
      z(ix,iy)=z(ix,iy)+(l+1-r)*conv(l)+(r-l)*conv(l+1)
1222  format(4i10,f15.8,"   print")
750   continue
751   continue
720   continue
c  **********************************
      do 60 l=1,np
      print 1001,(z(i,l),i=1,np)
1008  format(i10,"   z")
60    continue
      stop
      end
```


Figure B. File *lumpmdacl* provided parameters (center of the ellipse, radius, and incremental gravity) for four ellipses used in the experiment.

xl	*yl*	*al*	*bl*	*tl*	*gl*
0.	0.	0.90000	0.90000	0.	1.00000
0.	0.04425	0.85575	0.85575	0.	-1.00000
0.	0.04425	0.85425	0.85425	0.	1.00000
0.	0.	0.81000	0.81000	0.	-1.00000